XCO2 estimates from the OCO-2 measurements using a neural network approach

5   Leslie David, Francois-Marie Bréon, Frédéric Chevallier

Laboratoire des Sciences du Climat et de l'Environnement/IPSL,
CEA-CNRS-UVSQ, Université Paris-Saclay, F-91198 Gif-sur-Yvette, France
Correspondence to: Francois-Marie Breon (fmbreon@cea.fr)

10   **Abstract**. The OCO-2 instrument measures high-resolution spectra of the sun radiance reflected at the Earth surface or scattered in the atmosphere. These spectra are used to estimate the column integrated CO2 dry air mole fraction (XCO2) and the surface pressure. The official retrieval algorithm (NASA's Atmospheric CO2 Observations from Space retrievals - ACOS) uses a full physics algorithm and has been extensively evaluated. Here we propose an alternative approach based on an artificial neural network (NN) technique. For the training and evaluation, we use as a reference estimate the

15   surface pressures from a numerical weather model and the XCO2 derived from an atmospheric transport simulation constrained by surface air-sample measurements of CO2. The NN is trained here using real measurements acquired in nadir mode on cloud-free scenes during even months and is then evaluated against similar observations of odd months. The evaluation indicates that the NN retrieves the surface pressure with a root-mean-square error better than 3 hPa and XCO2 with a precision of 0.7 ppm. The statistics indicate that the NN, that has been trained with a representative set of

20   data, allows excellent accuracy, slightly better than that of the full physics algorithm. An evaluation against reference sunphotometer XCO2 retrievals indicates similar accuracy for the NN and ACOS estimates, with a skill that varies among the various stations. The NN-model differences show spatio-temporal structures that indicate a potential for improving our knowledge of CO2 fluxes. We finally discuss the pros and cons of using this NN approach for the processing of OCO-2 data.

1. Introduction

During the past decades, natural fluxes have absorbed about half of the anthropogenic emissions of CO2 (Knorr, 2009), but there is large uncertainty on the spatial distribution of this sink over time and therefore on the processes that control it. A growing network of high-precision atmospheric CO2 measurements has been used together with meteorological information to constrain the sources and sinks of CO2 using a technique known as *atmospheric inversion* (e.g., Peylin et

30   al., 2013), but the lack of data in large regions of the globe like the tropics does not allow monitoring these fluxes with enough space-time resolution. Early attempts to complement this network with satellite retrievals from sensors that were not specifically designed for this purpose were not successful (Chevallier et al., 2005), but a series of dedicated instruments have been put in orbit since the Greenhouse Gases Observing Satellite (GOSAT, Yokota et al., 2009) and the second Orbiting Carbon Observatory (OCO-2 Eldering et al., 2017a), launched in 2009 and 2014, respectively, and still

35   operated at the time of writing. This new and evolving constellation is directly supported by Japanese, US, Chinese and European space agencies (CEOS Atmospheric Composition Virtual Constellation Greenhouse Gas Team, 2018). All missions have adopted the same CO2 observation principle that consists in measuring the solar irradiance that has been

reflected at the Earth's surface in selected spectral bands. During the double atmospheric path (down-going and up-going), the sunlight is absorbed by atmospheric molecules at specific wavelengths. The resulting absorption lines on the measured

40   spectra makes it possible to estimate the amount of gas between the surface and the top of the atmosphere. CO_2 shows many such absorption lines around 1.61 and 2.06 µm that are used to estimate the CO_2 column. Similarly, the oxygen lines around 0.76 µm are used to estimate the surface pressure and can also be used to normalize the sunlight atmospheric path, leading to the column-average CO_2 dry air mole fraction, referred to as XCO2 (O'Brien and Rayner, 2002, Crisp et al., 2004).

45   One main difficulty in the retrieval of XCO2 from the measured spectra results from the presence of molecules that scatter light and change its atmospheric path. Accounting for aerosols, in particular, is challenging because aerosols are very variable in amount and in vertical distribution. Another major difficulty results from modelling errors. The radiative transfer models that are used for the retrieval leave significant residuals between the measured and modelled spectra, even after the XCO2 and aerosol amount have been optimized (Crisp et al., 2012; O'Dell et al., 2018). As a consequence of

50   the various uncertainties in the retrieval process, raw XCO2 retrievals show significant biases against reference ground-based retrievals (Wunch et al., 2011b, 2017). These biases, together with the comparison against modelling results, led to the development of empirical corrections to the retrieved XCO2. In the case of the OCO-2 v8 retrievals generated by NASA's Atmospheric CO_2 Observations from Space (ACOS), these corrections amount to roughly half that of the "signal", i.e. of the difference between the prior and the retrieved XCO2 (O'Dell et al. 2018).

55   The limitations in the full-physics retrieval method, despite considerable efforts and progresses (e.g., O'Dell et al. 2018, Reuter et al. 2017, Wu et al., 2018 in the case of OCO-2), encourages developing alternative approaches. Here, we want to re-evaluate the potential of an artificial neural network technique (NN) to estimate XCO2 from the measured spectra. A NN-based technique was already used by Chédin et al. (2003) for a fast retrieval of mid-tropospheric-mean CO_2 concentrations from some meteorological satellite radiometers. These authors trained their NNs on a large ensemble of

60   radiance simulations made by a reference radiation model and assuming diverse atmospheric and surface conditions. NN-based approaches are also commonly used for the retrieval of other species from various high-spectral-resolution satellite radiance measurements because of their computational efficiency (e.g., Hadji-Lazaro et al. 1999).

A neural network approach requires a large and comprehensive training dataset. A classical method for problems similar to that discussed here is to use a radiative transfer model and generate a large ensemble of pseudo observations based on

65   assumed atmospheric and surface parameters. However, as mentioned above, the radiative transfer models have deficiencies that are rather small, but nevertheless significant with respect to the high precision objective of the CO_2 measurements. We thus prefer to avoid using such radiative transfer models and rather base the training on a fully empirical approach (see, e.g., Aires et al., 2005). We use real OCO-2 observations together with collocated estimates of the surface pressure and XCO2. The retrievals from the NN approach are evaluated against model estimates of surface

70   pressure and XCO2, as well as observations from the Total Carbon Column Observing Network (TCCON, Wunch et al., 2011). The evaluation results show that the NN approach leads to estimates that are of similar quality as those from the official OCO-2 product. In the following, section 2 presents the approach while section 3 describes the results. Section 4 discusses the results and presents the way forward.

2.   Data and method

75   Our NN estimates XCO2 and the surface pressure from nadir spectra measured by the OCO-2 satellite over land. OCO-2 has eight cross-track footprints (e.g., Eldering et al., 2017), but we only use footprint #4 in the following for simplicity.

The focus on nadir measurements here is motivated by the complication introduced by the Doppler effect in glint mode, which is the other pointing mode for OCO-2 routine science operations: the absorption lines affect pixel elements that vary among the spectra. The solar lines in the nadir spectra are also affected by Doppler shifts due to the motion of the

80   Earth and satellite relative to the sun, but this concerns a limited set of spectral elements. The development of a glint-mode NN is therefore left for a future study.

We use spectral samples in the three bands of the instrument (around 0.76, 1.61 and 2.06 μm). They have footprints of ~ 3 km^2 on the ground. In principle, each band can be described by 1016 pixel elements but some are marked as bad either because some of the corresponding detectors died at some stage or because of known temporary or permanent issues. We

85   systematically remove 15 pixel elements that are flagged in about 80% of the spectra and 478 pixels in the band edges. Because the information in the spectrum is mostly in the relative depth of the absorption lines, and not in their overall amplitude, we normalize each spectrum by its maximum radiance value. This essentially removes the impact of the variations in the surface albedo and in the sun irradiance linked to the solar zenith angle.

As input to the NN, we add the viewing geometry (sun zenith angle and relative azimuth). The sun zenith angle drives

90   the atmospheric pathlength and is then required for the interpretation of the absorption line depth in terms of atmospheric optical depth. The azimuth was not included in our first attempts but it results, when included, in a significant improvement. Although, the NN technique does not allow for a clear physical interpretation, we assume that the information brought by the relative azimuth is linked to the polarization of the molecular scattering contribution to the measurements that varies with the azimuth.

95   The NN exploits these 2557 input variables to compute 2 variables only: XCO2 and the surface pressure. It is structured as a Multilayer Perceptron (Rumelhart et al. 1986) with one hidden layer of 500 neurons that use a sigmoid activation function. The weights of the input variables to the hidden neurons and the weights of the hidden variables to the output variables are adjusted iteratively with the standard Keras library (Chollet, 2015). The NN cost function becomes fairly constant for our evaluation set after about 100 iterations, while it continues to decrease for the training dataset, indicating

100   an over-fitting of the data. We thus stop the optimization after 100 iterations. Note that the NN estimate does not use any a-priori information on surface pressure or the CO2 profile after the training is done. Also, no explicit information is provided on the location or time period of the observation. The NN estimates are therefore only driven by the OCO-2 spectra measurements, together with the observation geometry.

The NN training is based on OCO-2 radiance measurements acquired during even months between January 2015 and

105   August 2018. The 4-year period allows varying the global background CO2 dry air mole fraction by ~ 2%, as much as typical XCO2 seasonal variations in the northern extra-tropics (see, e.g., Fig. 1 of Agustí-Panareda et al., 2019). Our evaluation dataset is based on observations during the odd months of the same period. In both cases, we make use of quality control filters of the ACOS v8 algorithm, i.e. we only use OCO-2 observations with a *warn level* lower or equal to 2, a cloud flag of 3 (very clear) and an *outcome flag* of 1. This choice is based on an evaluation of the surface pressure

110   estimates, that is described below (with the description of Figure 3). This distinction leads to 131 000 observations for the training and 155 000 for the evaluation.

For the reference surface pressure (training and evaluation), an obvious choice is the use of numerical weather analyses corrected for the pixel altitude. Indeed, the typical precision for surface pressure data is on the order of 1 ppm (Salstein et al. 2008). For convenience, we use the surface pressure that is provided together with the OCO-2 data and that is

115   derived from the Goddard Earth Observing System, Version 5, Forward Processing for Instrument Teams (GEOS5-FP-IT) created at Goddard Space Flight Center Global Modeling and Assimilation Office (Suarez et al. 2008 and Lucchesi

et al. 2013). There is no such obvious choice for XCO2 as there is no global-scale highly-accurate dataset of XCO2 and we thus rely here on best estimates from a modelling approach. We use the CO2 atmospheric inversion of the Copernicus Atmosphere Monitoring Service (CAMS, atmosphere.copernicus.eu, last access: 28 January 2020, Chevallier et al.,

120   2010); version 18r2). This product was released in July 2019 and contributed, e.g., to the Global Carbon Budget 2019 of Friedlingstein et al. (2019). It results from the assimilation of CO2 surface air-sample measurements in a global atmospheric transport model run at spatial resolution 1.90° in latitude and 3.75° in longitude over the period 1979-2018 and using the adjoint of this transport model. Neither satellite retrievals nor surface-based observations were used for this modelling. For each OCO-2 observations, XCO2 is computed from the collocated concentration vertical profile,

125   through a simple integration weighted by the pressure width of the model layers. The GEOS5-FP-IT surface pressure and the XCO2 from CAMS are used both for the training and the evaluation, although using independent datasets (odd and even months).

Many measured spectra lack one or several spectral pixels. This is particularly the case over South America, as a consequence of the South Atlantic cosmic flux anomaly that impacts the OCO-2 detector in this region. We therefore

130   devised a method to interpolate the spectra and fill the missing pixels. Our method first sorts all spectral pixels as a function of the measured radiance in a large number of complete measured spectra. The pixel ranks are averaged to generate a rank representative of the full dataset. Then, when a pixel element is missing in a spectrum, we look for its typical rank and we average the radiances of the two pixel elements that have the ranks just above and below. The procedure is applied even when several pixel elements are missing in a spectrum, except when these are successive in the

135   typical ranking. The procedure described here fills the missing elements, and the NN can then be applied to the corrected spectrum to estimate the surface pressure and XCO2.

3. Results

Figure 1 shows a density histogram of the GEOS5 FP-IT surface pressure analysis and of the NN estimate for the evaluation dataset (odd months). Clearly, there is an excellent agreement between the two over a very wide range of

140   surface pressures. There is no significant bias and the standard deviation is 2.7 hPa. The equivalent ACOS v9 retrieval shows a bias of 1.4 hPa and a standard deviation of 3.0 hPa, slightly larger than that of the NN approach. Note that the ACOS statistics are those of the ACOS retrieval-minus-prior statistics (see Section 2). Interpreting them in terms of error is counter-intuitive because the Bayesian retrieval is supposed to be better than the prior, but in practice radiation modelling errors lead to a different interpretation (see, e.g., the discussion in Section 4.3.4 of O'Dell et al. 2018).

145   Both NN and ACOS correlations with GEOS5 FP-IT are very high (0.998 and 0.997) although the best fit shows a very small deviation from the 1:1 line. Interestingly, the best fit deviations from the 1:1 line are of opposite sign (slopes 0.98 and 1.01). The results of the NN are surprisingly good given the simplicity of the approach and given that the NN estimate does not use any a-priori information or ancillary information such as the temperature profile. The quality of the NN results for the estimate of the surface pressure is a first demonstration of the potential of the approach. Note that the

150   retrieval accuracy holds over a very large range of surface pressure (the relative variations of XCO2 are much smaller), although there is some indication of biases for the lowest pressure that are under-represented in the training dataset.

Figure 2 is similar to Figure 1 but for XCO2. There is no significant bias between the NN estimate and the CAMS model, while the standard deviation is 0.74 ppm. The bias-corrected ACOS retrievals show a slight bias against the CAMS model and the standard deviation (0.93 ppm) is larger than that of the NN approach. Note that the statistics given here

155   are affected by CAMS modelling errors that may eventually be corrected with the help of the satellite information. The

best fit slope deviations from the 1:1 line are larger than for the surface pressure: the slopes are 0.94 for the NN and 0.95 for ACOS.

Figure 1 and 2, together with the quantitative assessment of the precision are given for the observations that are clear according to ACOS (Cloud Flag=3), that have a warn level of 2 or less, that may include missing pixel elements, and that have an outcome flag of 1 or 2. This choice is based on a prior performance analysis. We have analyzed how the performance of the NN approach varies with the quality indicators. For this objective, we have compared the retrieved surface pressure against the value derived from the numerical weather data, as in Figure 1, and we have evaluated the statistic of their difference as a function of the quality flags. First (figure not shown), there is no significant difference between cases when the measured spectra are complete and those when one or several missing pixel elements have been interpolated with the method described above. Conversely, the statistics vary with the cloud flag and the warn level, as shown in Figure 3. We only use the spectra for which an ACOS retrieval is available. Among those, about 53% are labeled as "very clear" while 43% are "probably clear". The statistics are slightly better for the former than they are for the latter. Conversely, the rather rare "definitely cloudy" and "probably cloudy" show deviations that are significantly larger. This result was well expected since our NN did not learn how to handle clouds in the spectra, so that all "definitely cloudy" and "probably cloudy" soundings are outside the domain covered by the training dataset. Most (78%) of the observations have a warn level of 0. The deviation statistics increase with the warn level, both in term of bias and standard deviation. In comparison the difference in the statistics for an outcome flag of 1 and 2 are small. Besides, more than half of the ACOS retrievals have an outcome flag of 2 which encourages us not to reject those for further use. Based on this analysis, we retain all spectra that are very clear (cloud flag of 3) and that have a warn level of 2 or less.

We have made a similar figure as Figure 3 but based on the XCO2 estimates (not shown). Although the results are similar in terms of sign (i.e. increase of the deviations with the warn levels), the signal is not as obvious (there is less relative difference between a warn level and another, or for the various cloud flags). Our interpretation is that the relative accuracy of the surface pressure that is used as a reference estimate is much better than that of the NN retrieval, whereas the accuracy of the XCO2 from CAMS is not much better than that of the NN. As a consequence, variations in the accuracy of the NN do not show up as clearly for XCO2 than they do for the surface pressure.

A classical method to evaluate an algorithm that estimates XCO2 from spaceborne observation is the comparison of its products against estimates from the TCCON network. These estimates use ground based solar absorption spectra recorded by Fourier Transform Infrared spectroscopy and have been tuned against airborne in-situ profiles (Wunch et al. 2010). To take advantage of the full potential of the TCCON network for the tuning and validation of the XCO2 estimates, the OCO-2 platform can be oriented so that the instrument field of view is close to the surface station. The ACOS full-physics algorithm can handle these spectra that are acquired in neither nadir nor glint geometries, but the NN was trained solely on nadir spectra and cannot be applied yet to the observations acquired in target mode. We thus have to rely on nadir measurements acquired in the vicinity of TCCON sites. In the following, we use nadir measurements that are within 5 degrees in longitude and 1.5 degrees in latitude to the TCCON site. The XCO2 estimates (either from ACOS, the NN, or the model sampled at the OCO-2 measurement location) are averaged for a given overpass. Only cases (overpasses) with at least 10 ACOS sample that meet the spatial criteria are kept. Similarly, we average the TCCON estimates of XCO2 within 30 minutes of the satellite overpass. The comparisons are shown in Figure 4 for each TCCON station of Table 1.

Two stations, Paris and Pasadena, show a large negative bias for both estimates, which may be interpreted as the impact of the city on the atmosphere sampled by the TCCON measurement, while the atmosphere sampled by the distant satellite may be less affected. Conversely, there is no such negative bias for other stations that are located close to large cities,

such as Tsukuba that is in the suburbs of the Tokyo Metropolitan area. Zugspitze is rather specific due to its high altitude. Note that there is no coincidence for the Lauder station due to the fact that most OCO-2 observations in the vicinity are acquired in Glint or Target modes. The comparison against TCCON indicates that the NN approach has a similar

200 performance as ACOS, if not better. The dispersion is larger for one versus the other for some stations, while the opposite is true for others. Note also that the CAMS model performs better than both satellite retrievals for most stations. This observation provides further justification to the use of this model for training the NN.

The evaluation of the algorithm performance is limited by the distance between the satellite estimate and its surface validation. This is inherent to the use of nadir-only observation that are seldom located close to the TCCON sites. A

205 reduction of the distance results in less coincidences, which leads to a validation dataset of poor representativeness.

We now investigate whether the model-minus-NN differences are purely random or contain some spatial or temporal structures. This question is important as, if the XCO2 differences do show some structures, they may be attributed to surface flux errors in the CAMS product that may then be corrected through inverse atmospheric modelling. Conversely, if the differences show a random structure, there is little hope to use these data to improve the surface fluxes used in the

210 CAMS product.

We first show (Figure 5) the difference between the NN estimate of the surface pressure and the surface pressure from the numerical weather analysis. These are monthly maps of the NN-minus-CAMS difference for the 3 years of the period at a 5°×5° resolution. We only present the odd months as the others months have been used for the training, and therefore do not show any significant differences. There are very clear spatial patterns of a few hPa which are not expected and

215 should be interpreted as a bias in the NN approach. In particular, positive biases tend to occur in the high latitudes, and negative biases toward the tropics. The structures show additional spatial and temporal patterns and are therefore more complex than just a latitude function. The same figure but based on the ACOS retrievals (Figure A1) display large-scale structures but with different spatial patterns: the surface pressure bias is mostly positive over the Northern latitudes and negative over the low latitudes. A histogram (Figure 6) of the monthly differences such as those shown on Figure 5

220 confirms that the amplitude of the surface pressure biases is larger with ACOS than it is with the NN. The NN (resp. ACOS) surface pressure bias is -0.13 hPa (resp 1.41 hPa) and the standard deviation is 2.37 (resp. 2.76 hPa).

Figure 7 is similar as Figure 5 but for XCO2 difference between the NN estimate and the CAMS model. As for the surface pressure, there are clear spatial patterns, with amplitudes of 1 to 2 ppm. The question is whether these are mostly linked to monthly biases in the CAMS model or to the NN. The first hypothesis is of course more favorable as it would

225 indicate that the satellite data can bring new information to constrain the surface fluxes. However, the analysis of the surface pressure suggests that the NN may show biases with spatially coherent patterns. Interestingly, the patterns vary in time and are not correlated with those of the surface pressure.

The differences of ACOS estimates to the CAMS model also show patterns of similar amplitude as those in Figure 7 (Figure A2). However, there is no clear correspondence between these patterns and those obtained using the NN product.

230 The differences between the satellite products and the CAMS model are small, but these contain the information that may be used to improve our knowledge on the surface fluxes. The absence of clear correlation between the spatio-temporal pattern from the NN and ACOS approaches indicate that their use would lead to very different corrections on the surface fluxes, if used as input of an atmospheric inversion approach. Figure 6, top, shows the histogram of these monthly mean differences. The histograms are very similar for the two satellite products, although the standard deviation of the

235 difference to the CAMS model is slightly larger for ACOS than it is for the NN approach (0.89 vs 0.82 ppm).

4. Discussion and Conclusion

The results shown above indicate that the NN approach allows an estimate of surface pressure and XCO2 with a precision that is similar or better than that of the operational ACOS algorithm. The lack of independent "truth" data does not allow a full evaluation of the product precision. However, there are indications that the precision on the surface pressure is better than 3 ppm, while that of XCO2 is better than 0.8 ppm. Indeed, the data used for the product evaluation has its own error that is difficult to disentangle from that of the estimate based on the satellite observation.

One obvious advantage of the NN approach is the speed of the computation that is several orders of magnitude higher than that of the full physics algorithm. This is significant given the current re-processing time of the OCO-2 dataset despite the considerable computing power that is made available for the mission. It also bears interesting prospects for future XCO2 imaging missions that will bring even higher data volume (e.g., Pinty et al., 2017).

Another advantage is that the NN approach as shown in this paper does not require the extensive de-bias procedure which is necessary for the ACOS product (O'Dell et al 2018, Kiel et al. 2019). Per construction, there is no bias between the NN estimates and the dataset that is used for the NN training. The NN approach requires therefore less effort and manpower.

There are however a number of drawbacks for the NN approach that is described in this paper.

One obvious drawback is the use of a CO2 model simulation in the training while the main purpose of the satellite observation is to improve our current knowledge on atmospheric CO2 and its surface fluxes. Our argument is that, although the CAMS simulation used here has high skill (as demonstrated in Figure 4), it may have positive or negative XCO2 biases for some months and some areas. These biases are independent from the measured spectra so that the NN training will aim at average values. As a consequence, the NN product could in principle be of higher quality than the CAMS product, even though the same model has been used as the reference estimate for the training (see, e.g., Aires et al., 2005).

Another drawback of the NN approach is that it does not provide an averaging kernel. The NN is trained to retrieve a straight pressure-weighted total column but the output does not provide any information on the true vertical sensitivity of the radiances. When comparing with model simulations, for instance for atmospheric inversion, one option would be to use a weighting that is homogeneous over the vertical, as this is the product that the NN was trained to simulate. Another option would be to use typical averaging kernels of the full physics algorithm as the vertical sensitivity of the measurement impacts similarly the NN and the ACOS products.

We acknowledge the fact that the NN product that is evaluated here is not fully independent from the ACOS product. Indeed, we use the cloud flag and the quality diagnostic from ACOS to select the spectra that are of sufficient quality. If we aim at some kind of operational product, there is a need to design a procedure to identify these good quality spectra. One option would be to compare the surface pressure retrieved by the NN to the numerical weather data estimate, and to reject cases with significant deviations (e.g. differences larger than 3 hPa).

Despite these drawbacks, the results shown in this paper do show that a neural network has a large potential for the estimate of XCO2 from satellite observations such as those of OCO-2, the forthcoming MicroCarb (Pascal et al. 2017) or the CO2M constellation (Sierk et al. 2018) that aims at measuring anthropogenic emissions. It is rather amazing that a first attempt leads to trueness and precision numbers that are similar or better than those of the full physics algorithm. There are several ways for improvement: one is to provide the NN with some ancillary information such as the surface altitude or a proxy of the atmospheric temperature. Another one is to train the NN with model estimates (such as those

275 of CAMS used here) but that have been better sampled for their assumed precision, for instance through a multi-model evaluation. Also, one could train the NN with observations acquired during a few days of each month, rather than the even months as done here, so that the evaluation dataset would provide a better evaluation of the seasonal cycle.

Our next objective is to attempt a similar NN approach but for the measurements that have been acquired in the glint mode. As explained above, the glint observations may be more difficult to reproduce by the NN than those acquired in
280 the nadir mode. However, we have been very much surprised by the ability of the NN with the nadir data, and cannot exclude to be surprised again. Last, we shall analyze the spatial structure of the NN retrievals in regions that are expected to be homogeneous and in regions where structures of anthropogenic origin are expected (e.g., Reuter et al., 2019).

Acknowledgments

This work was in part funded by CNES, the French space agency, in the context of the preparation for the MicroCarb
285 mission. OCO-2 L1 and L2 data were produced by the OCO-2 project at the Jet Propulsion Laboratory, California Institute of Technology, and obtained from the ACOS/OCO-2 data archive maintained at the NASA Goddard Earth Science Data and Information Services Center. TCCON data were obtained from the TCCON Data Archive, hosted by the Carbon Dioxide Information Analysis Center (CDIAC) - tccon.onrl.gov. We warmly thank those who made these data available.

References

290 Agustí-Panareda, A., Diamantakis, M., Massart, S., Chevallier, F., Muñoz-Sabater, J., Barré, J., Curcoll, R., Engelen, R., Langerock, B., Law, R. M., Loh, Z., Morguí, J. A., Parrington, M., Peuch, V.-H., Ramonet, M., Roehl, C., Vermeulen, A. T., Warneke, T., and Wunch, D.: Modelling CO_2 weather – why horizontal resolution matters, *Atmos. Chem. Phys.*, 19, 7347–7376, https://doi.org/10.5194/acp-19-7347-2019, 2019.

Aires, F., C. Prigent, and W. B. Rossow (2005), Sensitivity of satellite microwave and infrared observations to soil
295 moisture at a global scale: 2. Global statistical relationships, *J. Geophys. Res.*, 110, D11103, doi:10.1029/2004JD005094.

CEOS Atmospheric Composition Virtual Constellation Greenhouse Gas Team: A constellation architecture for monitoring carbon dioxide and methane from space, Report from the Committee on Earth Observation Satellites (CEOS) Atmospheric Composition Virtual Constellation (AC-VC), available at: http://ceos.org/document_management/Virtual_Constellations/ACC/Documents/CEOS_AC-
300 VC_GHG_White_Paper_Version_1_20181009.pdf, 2018.

Chédin, A., S. Serrar, N. A. Scott, C. Crévoisier, and R. Armante (2003b), First global measurement of midtropospheric CO_2 from NOAA polar satellites: Tropical zone, *J. Geophys. Res.*, 108(D2), 4581, doi:10.1029/2003JD003439.

Chevallier, F., Fisher, M., Peylin, P., Serrar, S., Bousquet, P., Bréon, F.-M., Chédin, A., and Ciais, P.: Inferring CO_2 sources and sinks from satellite observations: Method and application to TOVS data, *J. Geophys. Res.*, 110,
305 D24309, https://doi.org/10.1029/2005JD006390, 2005.

Chevallier, F., Ciais, P., Conway, T. J., Aalto, T., Anderson, B. E., Bousquet, P., Brunke, E. G., Ciattaglia, L., Esaki, Y., Frohlich, M., Gomez, A., Gomez-Pelaez, A. J., Haszpra, L., Krummel, P. B., Langenfelds, R. L., Leuenberger, M., Machida, T., Maignan, F., Matsueda, H., Morgu, J. A., Mukai, H., Nakazawa, T., Peylin, P., Ramonet, M., Rivier, L., Sawa, Y., Schmidt, M., Steele, L. P., Vay, S. A., Vermeulen, A. T., Wofsy, S., and Worthy, D.: CO2 surface fluxes at
310 grid point scale estimated from a global 21 year reanalysis of atmo- spheric measurements, *J. Geophys. Res.-Atmos.*, 115, D21307, https://doi.org/10.1029/2010JD013887, 2010.

Chollet F et al. (2015) Keras developer guides, https://keras.io/guides/. Last accessed June 1st, 2020

Crisp, D., Atlas, R. M., Breon, F.-M., Brown, L. R., Burrows, J. P., Ciais, P., Connor, B. J., Doney, S. C., Fung, I. Y., Jacob, D. J., Miller, C. E., O'Brien, D., Pawson, S., Randerson, J. T., Rayner, P., Salawitch, R. J., Sander, S. P., Sen, B.,
315 Stephens, G. L., Tans, P. P., Toon, G. C., Wennberg, P. O., Wofsy, S. C., Yung, Y. L., Kuang, Z., Chudasama, B., Sprague, G., Weiss, B., Pollock, R., Kenyon, D., and Schroll, S.: The Orbiting Carbon Observatory (OCO) mission, *Adv. Space Res.*, 34, 700–709, doi:10.1016/j.asr.2003.08.062, 2004.

Crisp, D., Fisher, B. M., O'Dell, C., Frankenberg, C., Basilio, R., Bösch, H., Brown, L. R., Castano, R., Connor, B., Deutscher, N. M., Eldering, A., Griffith, D., Gunson, M., Kuze, A., Mandrake, L., McDuffie, J., Messerschmidt, J., Miller,

320   Deutscher, N., N. M., Diao, M., Elkins, J. W., Gerbig, C., Gottlieb, E., Griffith, D. W. T., Hurst, D. F., Jiménez, R., Keppel-Aleks, G., Kort, E. A., Macatangay, R., Machida, T., Matsueda, H., Moore, F., Morino, I., Park, S., Robinson, J., Roehl, C. M., Sawa, Y., Sherlock, V., Sweeney, C., Tanaka, T., and Zondlo, M. A.: Calibration of the Total Carbon Column Observing Network using aircraft profile data, *Atmos. Meas. Tech.*, 3, 1351–1362, https://doi.org/10.5194/amt-3-1351-2010, 2010.

325   Deutscher, N., J. Notholt, J. Messerschmidt, C. Weinzierl, T. Warneke, C. Petri, P. Grupe, K. Katrynski. 2017. TCCON data from Bialystok, Poland, Release GGG2014R2. TCCON data archive, hosted by CaltechDATA, California Institute of Technology, Pasadena, CA, U.S.A. http://doi.org/10.14291/tccon.ggg2014.bialystok01.R2

Eldering, A., R. Pollock, R. Lee, R. Rosenberg, F. Oyafuso, D. Crisp, R. Granat (2015), Orbiting Carbon Observatory (OCO)-2, Level 1B theoretical basis document (2015),Version 1.2, 40 pp. , http://disc.sci.gsfc.nasa.gov/OCO-
330   2/documentation/oco-2-v6/OCO2_L1B%20ATBD.V6.pdf

Eldering, A., P. O. Wennberg, D. Crisp, D. Schimel, M. R. Gunson, A. Chatterjee, J. Liu, F. M. Schwandner, Y. Sun, C. W. O'Dell, C. Frankenberg, T. Taylor, B. Fisher, G. B.Osterman, D. Wunch, J. Hakkarainen, J. Tamminen, B. Weir, The Orbiting Carbon Observatory-2 early science investigations of regional carbon dioxide fluxes, *Science*, 358 (2017). DOI: 10.1126/science.aam5745

335   Friedlingstein, P., Jones, M. W., O'Sullivan, M., Andrew, R. M., Hauck, J., Peters, G. P., Peters, W., Pongratz, J., Sitch, S., Quéré, C. L., Bakker, D. C. E., Canadell, J. G., Ciais, P., Jackson, R. B., Anthoni, P., Barbero, L., Bastos, A., Bastrikov, V., Becker, M., Bopp, L., Buitenhuis, E., Chandra, N., Chevallier, F., Chini, L. P., Currie, K. I., Feely, R. A., Gehlen, M., Gilfillan, D., Gkritzalis, T., Goll, D. S., Gruber, N., Gutekunst, S., Harris, I., Haverd, V., Houghton, R. A., Hurtt, G., Ilyina, T., Jain, A. K., Joetzjer, E., Kaplan, J. O., Kato, E., Klein Goldewijk, K., Korsbakken, J. I., Landschützer, P.,
340   Lauvset, S. K., Lefèvre, N., Lenton, A., Lienert, S., Lombardozzi, D., Marland, G., McGuire, P. C., Melton, J. R., Metzl, N., Munro, D. R. Nabel, J. E. M. S., Nakaoka, S.-I., Neill, C., Omar, A. M., Ono, T., Peregon, A., Pierrot, D., Poulter, B., Rehder, G., Resplandy, L., Robertson, E., Rödenbeck, C., Séférian, R., Schwinger, J., Smith, N., Tans, P. P., Tian, H., Tilbrook, B., Tubiello, F. N., Werf, G. R. van der, Wiltshire, A. J. and Zaehle, S.: Global Carbon Budget 2019, *Earth System Science Data*, 11(4), 1783–1838, doi:https://doi.org/10.5194/essd-11-1783-2019, 2019.

345   Griffith, D. W. T., V. A. Velazco, N. Deutscher, C. Murphy, N. Jones, S. Wilson, R. Macatangay, G. Kettlewell, R. R. Buchholz, M. Riggenbach. 2017. TCCON data from Wollongong, Australia, Release GGG2014R0. TCCON data archive, hosted by CaltechDATA, California Institute of Technology, Pasadena, CA, U.S.A. https://doi.org/10.14291/tccon.ggg2014.wollongong01.R0/1149291

Griffith, D. W. T., N. Deutscher, V. A. Velazco, P. O. Wennberg, Y. Yavin, G. Keppel Aleks, R. Washenfelder, G. C.
350   Toon, J.-F. Blavier, C. Murphy, N. Jones, G. Kettlewell, B. Connor, R. Macatangay, C. Roehl, M. Ryczek, J. Glowacki, T. Culgan, G. Bryant. 2017. TCCON data from Darwin, Australia, Release GGG2014R0. TCCON data archive, hosted by CaltechDATA, California Institute of Technology, Pasadena, CA, U.S.A. http://doi.org/10.14291/tccon.ggg2014.darwin01.R0/1149290

Hadji-Lazaro, J., C. Clerbaux, and S. Thiria, an inversion algorithm using neural networks to retrieve atmospheric CO
355   total columns from high-resolution nadir radiances, *J. Geophys. Res.*, 104, 23,841-23,854, 199

Hase, F., T. Blumenstock, S. Dohe, J. Gross, M. Kiel. 2017. TCCON data from Karlsruhe, Germany, Release GGG2014R1. TCCON data archive, hosted by CaltechDATA, California Institute of Technology, Pasadena, CA, U.S.A. https://doi.org/10.14291/tccon.ggg2014.karlsruhe01.R1/1182416

Iraci, L., J. Podolske, P. Hillyard, C. Roehl, P. O. Wennberg, J.-F. Blavier, J. Landeros, N. Allen, D. Wunch, J. Zavaleta,
360   E. Quigley, G. Osterman, R. Albertson, K. Dunwoody, H. Boyden. 2017. TCCON data from Armstrong Flight Research Center, Edwards, CA, USA, Release GGG2014R1. TCCON data archive, hosted by CaltechDATA, California Institute of Technology, Pasadena, CA, U.S.A. https://doi.org/10.14291/tccon.ggg2014.edwards01.R1/1255068

Kiel, M., O'Dell, C. W., Fisher, B., Eldering, A., Nassar, R., MacDonald, C. G., and Wennberg, P. O.: How bias correction goes wrong: measurement of XCO2 affected by erroneous surface pressure estimates, *Atmos. Meas. Tech.*, 12, 2241–
365   2259, https://doi.org/10.5194/amt-12-2241-2019, 2019.

Kivi, R., P. Heikkinen, E. Kyro. 2017. TCCON data from Sodankyla, Finland, Release GGG2014R0. TCCON data archive, hosted by CaltechDATA, California Institute of Technology, Pasadena, CA, U.S.A. https://doi.org/10.14291/tccon.ggg2014.sodankyla01.R0/1149280

Knorr, W. (2009), Is the airborne fraction of anthropogenic CO2 emissions increasing? *Geophys. Res. Lett.*, 36, L21710,
370   doi:10.1029/2009GL040613.

Liu C., Wang, W., Sun, Y. 2018. TCCON data from Hefei, China, Release GGG2014R0. TCCON data archive, hosted by CaltechDATA, California Institute of Technology, Pasadena, CA, U.S.A. http://dx.doi.org/10.14291/tccon.ggg2014.hefei01.R0

375   Lucchesi, R.: File Specification for GEOS-5 FP-IT (Forward Processing for Instrument Teams), Tech. rep., NASA Goddard Spaceflight Center, Greenbelt, MD, USA, available at: https: //ntrs.nasa.gov/archive/nasa/casi.ntrs.nasa.gov/20150001438.pdf (last access: 4 December 2018), 2013.

Morino, I., T. Matsuzaki, A. Shishime. 2017. TCCON data from Tsukuba, Ibaraki, Japan, 125HR, Release GGG2014R2. TCCON data archive, hosted by CaltechDATA, California Institute of Technology, Pasadena, CA, U.S.A. http://doi.org/10.14291/tccon.ggg2014.tsukuba02.R2

380   Morino, I., Natraj, V., Notholt, J., O'Brien, D. M., Oyafuso, F., Polonsky, I., Robinson, J., Salawitch, R., Sherlock, V., Smyth, M., Suto, H., Taylor, T. E., Thompson, D. R., Wennberg, P. O., Wunch, D., and Yung, Y. L.: The ACOS CO2 retrieval algorithm – Part II: Global XCO2 data characterization, *Atmos. Meas. Tech.*, 5, 687– 707, https://doi.org/10.5194/amt-5-687-2012, 2012.

Notholt, J., C. Petri, T. Warneke, N. Deutscher, M. Buschmann, C. Weinzierl, R. Macatangay, P. Grupe. 2017. TCCON
385   data from Bremen, Germany, Release GGG2014R0. TCCON data archive, hosted by CaltechDATA, California Institute of Technology, Pasadena, CA, U.S.A. https://doi.org/10.14291/tccon.ggg2014.bremen01.R0/1149275

O'Brien, D. M. and Rayner, P. J.: Global observations of the carbon budget 2. CO2 column from differential absorption of reflected sunlight in the 1.61 μm band of CO2, *J. Geophys. Res.*, 107, ACH6-1, doi:10.1029/2001JD000617, 2002.

O'Dell, C. W., Eldering, A., Wennberg, P. O., Crisp, D., Gunson, M. R., Fisher, B., Frankenberg, C., Kiel, M., Lindqvist,
390   H., Mandrake, L., Merrelli, A., Natraj, V., Nelson, R. R., Osterman, G. B., Payne, V. H., Taylor, T. E., Wunch, D., Drouin, B. J., Oyafuso, F., Chang, A., McDuffie, J., Smyth, M., Baker, D. F., Basu, S., Chevallier, F., Crowell, S. M. R., Feng, L., Palmer, P. I., Dubey, M., García, O. E., Griffith, D. W. T., Hase, F., Iraci, L. T., Kivi, R., Morino, I., Notholt, J., Ohyama, H., Petri, C., Roehl, C. M., Sha, M. K., Strong, K., Sussmann, R., Te, Y., Uchino, O., and Velazco, V. A.: Improved retrievals of carbon dioxide from Orbiting Carbon Observatory-2 with the version 8 ACOS algorithm, *Atmos.*
395   *Meas. Tech.*, 11, 6539–6576, https://doi.org/10.5194/amt-11-6539-2018, 2018.

Pascal, V., Buil, C., Loesel, J., Tauziede, L., Jouglet, D., and Buisson, F.: An improved microcarb dispersive instrumental concept for the measurement of greenhouse gases concentration in the atmosphere, *Proc. SPIE* 10563, 10563K-1– 10563K-9, https://doi.org/10.1117/12.2304219, 2017.

Peylin, P., Law, R. M., Gurney, K. R., Chevallier, F., Jacobson, A. R., Maki, T., Niwa, Y., Patra, P. K., Peters, W.,
400   Rayner, P. J., Rödenbeck, C., van der Laan-Luijkx, I. T., and Zhang, X.: Global atmospheric carbon budget: results from an ensemble of atmospheric CO₂ inversions, *Biogeosciences*, 10, 6699–6720, https://doi.org/10.5194/bg-10-6699-2013, 2013.

Pinty, B., G. Janssens-Maenhout, M. Dowell, H. Zunker, T. Brunhes, P. Ciais, D. Dee, H. Denier van der Gon, H. Dolman, M. Drinkwater, R. Engelen, M. Heimann, K. Holmlund, R. Husband, A. Kentarchos, Y. Meijer, P. Palmer and M. Scholze
405   (2017) An operational anthropogenic CO₂ emissions monitoring & verification support capacity - Baseline requirements, Model components and functional architecture, doi:10.2760/39384, European Commission Joint Research Centre, EUR 28736 EN

Reuter, M.; Buchwitz, M.; Schneising, O.; Noël, S.; Rozanov, V.; Bovensmann, H.; Burrows, J.P. A Fast Atmospheric Trace Gas Retrieval for Hyperspectral Instruments Approximating Multiple Scattering—Part 1: Radiative Transfer and a
410   Potential OCO-2 XCO2 Retrieval Setup. Remote Sens. 2017, 9, 1159.

Reuter, M., Buchwitz, M., Schneising, O., Krautwurst, S., O'Dell, C. W., Richter, A., Bovensmann, H., and Burrows, J. P.: Towards monitoring localized CO₂ emissions from space: co-located regional CO₂ and NO₂ enhancements observed by the OCO-2 and S5P satellites, Atmos. Chem. Phys., 19, 9371–9383, https://doi.org/10.5194/acp-19-9371-2019, 2019.

Rumelhart, D. E., G. E. Hinton, and R. J. Williams (1986), Learning internal representations by error propagation. Parallel
415   Distributed Processing: Explorations in the Microstructure of Cognition 1, D. E. Rumelhart and J. L. McClelland, Eds., The MIT Press, 318–362.

Salstein, D. A., Ponte, R. M., and Cady-Pereira, K.: Uncertainties in atmospheric surface pressure fields from global analyses, *J. Geophys. Res.*, 113, D14107, https://doi.org/10.1029/2007JD009531, 2008.

Shiomi, K., Kawakami, S., H. Ohyama, K. Arai, H. Okumura, C. Taura, T. Fukamachi, M. Sakashita. 2017. TCCON data
420   from Saga, Japan, Release GGG2014R0. TCCON data archive, hosted by CaltechDATA, California Institute of Technology, Pasadena, CA, U.S.A. https://doi.org/10.14291/tccon.ggg2014.saga01.R0/1149283

Sierk, B., Bézy, J.-L., Löscher, A., and Meijer, Y.: TheEuropean CO2 Monitoring Mission: Observing anthropogenic greenhouse gas emissions from space, International Conference on Space Optics, SPIE, 237–250, https://doi.org/10.1117/12.2535941, 2018.

425   Suarez, M. J., Rienecker, M. M., Todling, R., Bacmeister, J., Takacs, L., Liu, H. C., Gu, W., Sienkiewicz, M., Koster, R. D., and Gelaro, R.: The GEOS-5 Data Assimilation System-Documentation of Versions 5.0.1, 5.1.0, and 5.2.0, Tech. rep., NASA Goddard Spaceflight Center, Greenbelt, MD, USA, available at: https://ntrs.nasa.gov/archive/nasa/casi.ntrs. nasa.gov/20120011955.pdf (last access: 4 December 2018), 2008.

430   Sussmann, R., M. Rettinger. 2017. TCCON data from Garmisch, Germany, Release GGG2014R2. TCCON data archive, hosted by CaltechDATA, California Institute of Technology, Pasadena, CA, U.S.A. https://doi.org/10.14291/tccon.ggg2014.garmisch01.R2

Te, Y., P. Jeseck, C. Janssen. 2017. TCCON data from Paris, France, Release GGG2014R0. TCCON data archive, hosted by CaltechDATA, California Institute of Technology, Pasadena, CA, U.S.A. https://doi.org/10.14291/tccon.ggg2014.paris01.R0/1149279

435   Warneke, T., J. Messerschmidt, J. Notholt, C. Weinzierl, N. Deutscher, C. Petri, P. Grupe, C. Vuillemin, F. Truong, M. Schmidt, M. Ramonet, E. Parmentier. 2017. TCCON data from Orleans, France, Release GGG2014R1. TCCON data archive, hosted by CaltechDATA, California Institute of Technology, Pasadena, CA, U.S.A. https://doi.org/10.14291/tccon.ggg2014.orleans01.R1

Wennberg, P. O., D. Wunch, C. Roehl , J.-F. Blavier, G. C. Toon, N. Allen. 2017. TCCON data from California Institute
440   of Technology, Pasadena, California, USA, Release GGG2014R1. TCCON data archive, hosted by CaltechDATA, California Institute of Technology, Pasadena, CA, U.S.A. https://doi.org/10.14291/tccon.ggg2014.pasadena01.R1/1182415

Wennberg, P. O., D. Wunch, C. Roehl, J.-F. Blavier, G. C. Toon, N. Allen, P. Dowell, K. Teske, C. Martin, J. Martin. 2017. TCCON data from Lamont, Oklahoma, USA, Release GGG2014R1. TCCON data archive, hosted by
445   CaltechDATA, California Institute of Technology, Pasadena, CA, U.S.A. https://doi.org/10.14291/tccon.ggg2014.lamont01.R1/1255070

Wennberg, P. O., C. Roehl, D. Wunch, G. C. Toon, J.-F. Blavier, R. Washenfelder, G. Keppel-Aleks, N. Allen, J. Ayers. 2017. TCCON data from Park Falls, Wisconsin, USA, Release GGG2014R1. TCCON data archive, hosted by CaltechDATA, California Institute of Technology, Pasadena, CA, U.S.A.
450   http://doi.org/10.14291/tccon.ggg2014.parkfalls01.R1

Wu, L., Hasekamp, O., Hu, H., Landgraf, J., Butz, A., aan de Brugh, J., Aben, I., Pollard, D. F., Griffith, D. W. T., Feist, D. G., Koshelev, D., Hase, F., Toon, G. C., Ohyama, H., Morino, I., Notholt, J., Shiomi, K., Iraci, L., Schneider, M., de Mazière, M., Sussmann, R., Kivi, R., Warneke, T., Goo, T.-Y., and Té, Y.: Carbon dioxide retrieval from OCO-2 satellite observations using the RemoTeC algorithm and validation with TCCON measurements, Atmos. Meas. Tech., 11, 3111–
455   3130, https://doi.org/10.5194/amt-11-3111-2018, 2018.

Wunch, D., G.C. Toon, J.-F.L. Blavier, R.A. Washenfelder, J. Notholt, B.J. Connor, D.W.T. Griffith, V. Sherlock, P.O. Wennberg. The Total Carbon Column Observing Network. *Phil. Trans. R. Soc.* A (2011a) 369, doi:10.1098/rsta.2010.0240

Wunch, D., Wennberg, P. O., Toon, G. C. et al. (2011b), A method for evaluating bias in global measurements of CO_2
460   total columns from space. *Atmos. Chem. Phys.*, 11, 12317-12337.

Wunch, D., Wennberg, P. O., Osterman, G., Fisher, B., Naylor, B., Roehl, C. M., O'Dell, C., Mandrake, L., Viatte, C., Kiel, M., Griffith, D. W. T., Deutscher, N. M., Velazco, V. A., Notholt, J., Warneke, T., Petri, C., De Maziere, M., Sha, M. K., Sussmann, R., Rettinger, M., Pollard, D., Robinson, J., Morino, I., Uchino, O., Hase, F., Blumenstock, T., Feist, D. G., Arnold, S. G., Strong, K., Mendonca, J., Kivi, R., Heikkinen, P., Iraci, L., Podolske, J., Hillyard, P. W., Kawakami,
465   S., Dubey, M. K., Parker, H. A., Sepulveda, E., García, O. E., Te, Y., Jeseck, P., Gunson, M. R., Crisp, D., and Eldering, A.: Comparisons of the Orbiting Carbon Observatory-2 (OCO-2) XCO2 measurements with TCCON, *Atmos. Meas. Tech.*, 10, 2209–2238, https://doi.org/10.5194/amt10-2209-2017, 2017.

Wunch, D., Toon, G. C., Wennberg, P. O., Wofsy, S. C., Stephens, B. B., Fischer, M. L., Uchino, O., Abshire, J. B., Bernath, P., Biraud, S. C., Blavier, J.-F. L., Boone, C., Bowman, K. P., Browell, E. V., Campos, T., Connor, B. J., Daube,
470   Yokota, T., Yoshida, Y., Eguchi, N., Ota, Y., Tanaka, T., Watanabe, H., and Maksyutov, S.: Global Concentrations of CO2 and CH4 Retrieved from GOSAT: First Preliminary Results, SOLA, 5, 160–163, 2009.

Zhou, M., Dils, B., Wang, P., Detmers, R., Yoshida, Y., O'Dell, C. W., Feist, D. G., Velazco, V. A., Schneider, M., and De Mazière, M. (2016), Validation of TANSO-FTS/GOSAT XCO2 and XCH4 glint mode retrievals using TCCON data from near-ocean sites, *Atmos. Meas. Tech.*, 9, 1415-1430, doi:10.5194/amt-9-1415-2016.

475

Figures and Tables
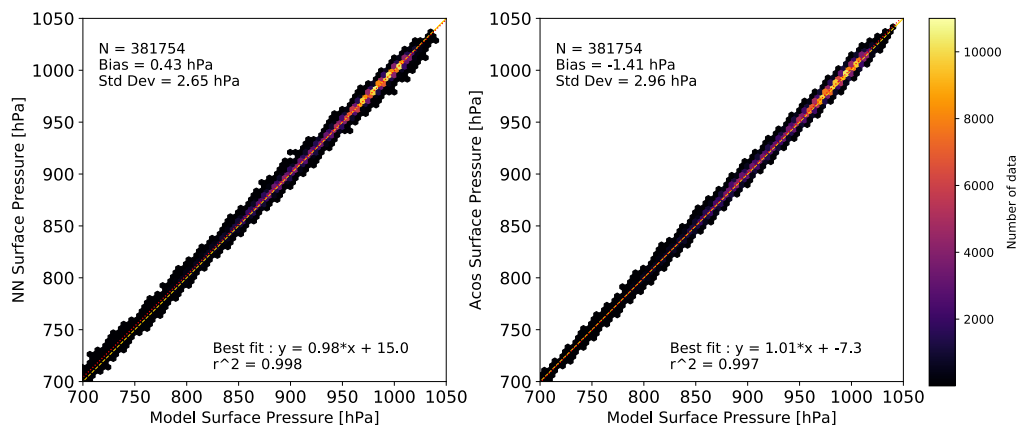
Figure 1: Density histogram of the surface pressure retrieved from the OCO-2 satellite measurements against that derived from GEOS-FP-IT. The left figure is for the NN approach while the right figure is for the ACOS v9 retrieval (using the official bias-correction). The figure insets provide the number of data points, the bias, the standard deviation, the equation of the best linear fit and the correlation.

480
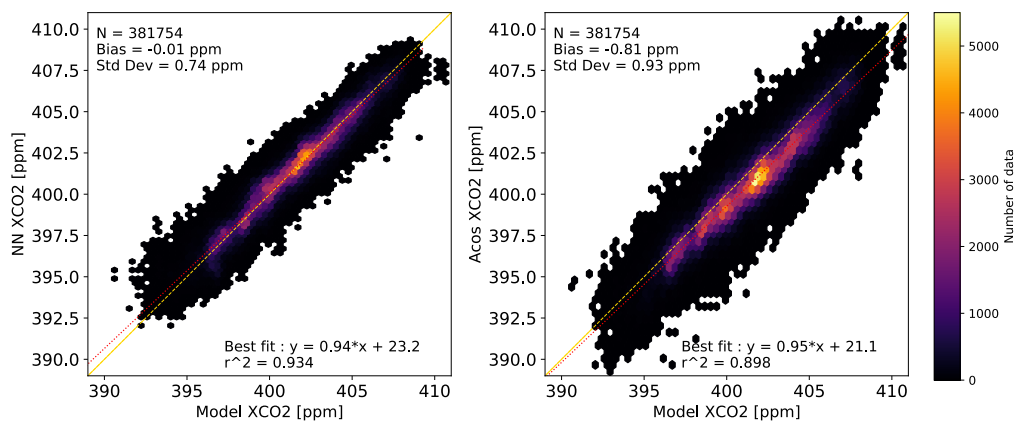
485   **Figure 2**: Same as Figure 1 but for XCO2. In this case, the reference data is the CAMS v18r2 simulation.
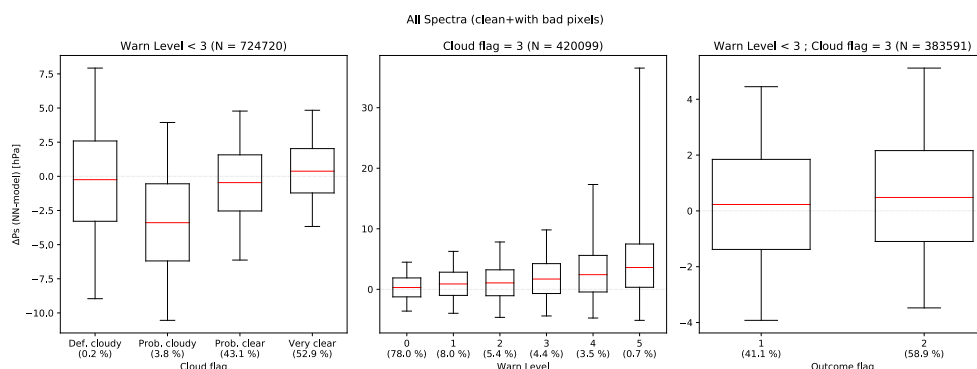
Figure 3: Statistics on the difference between the surface pressure retrieved by the NN approach and that derived from the numerical weather data, as a function of various quality parameters. In these figures, the red line is the median, the boxes indicate the 25 and 75% percentiles and the whiskers indicate the 5-95% range. The left figure shows the statistics as a function of the cloud flag, the middle figure is as a function of the warn level, while the right figure is as a function of the outcome flag.
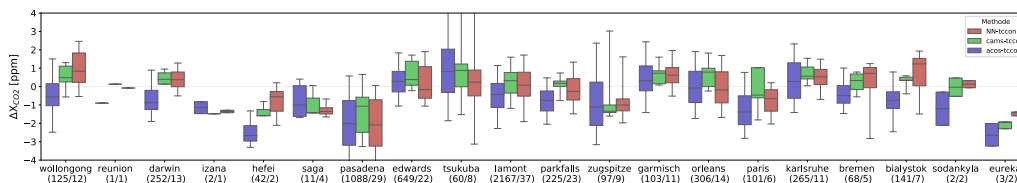
Figure 4: Statistics of the differences between the NN retrieval (red), the CAMS model (green) or the bias-corrected ACOS retrievals (blue) and the TCCON retrievals. The boxes indicate the 25-75% percentiles and the median is shown by the horizontal line within the box. The whiskers indicate the 5-95% percentiles. Stations are ordered by increasing latitudes. The numbers below the station name indicate the number of individual observations and coincidence days used for the statistics. Reference to the TCCON observations are provided in table 1.
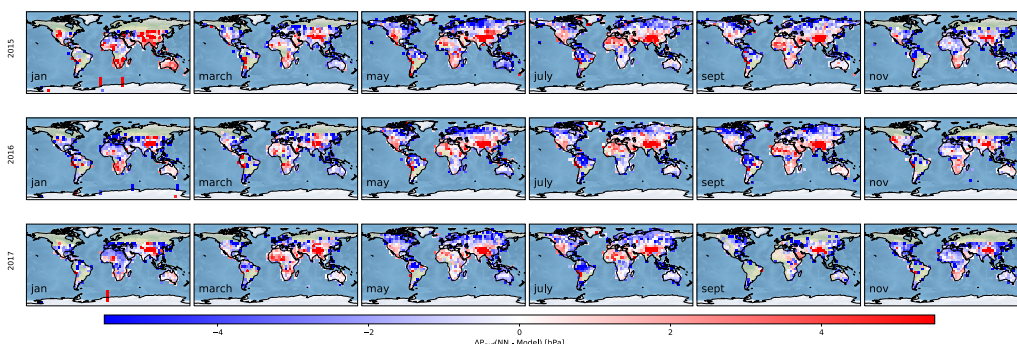
Figure 5: Difference between the NN estimate of the surface pressure and the numerical weather analysis. The differences have been averaged at monthly and spatial 5°×5° resolutions. The results are shown for 3 years and only for the months that were not used for the training.

505
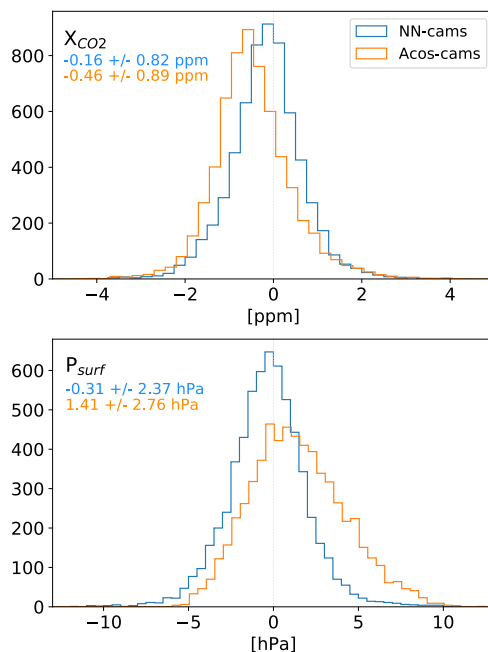
Figure 6: Histogram of the monthly mean differences, at 5° resolution (such as those shown in Figure 5), between the satellite retrievals and the CAMS model. The top figure is for XCO2 while the bottom figure is for the surface pressure. The blue line is for the NN product while the orange line is for ACOS.

510
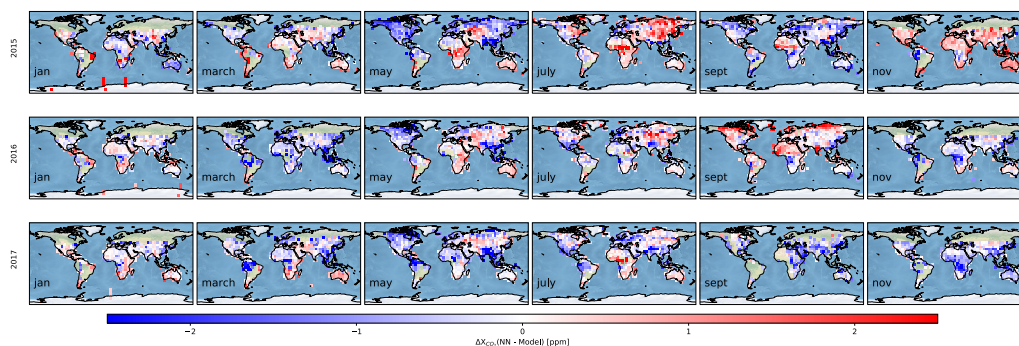
Figure 7: Same as Figure 5 but for the difference between the XCO2 estimated by the NN approach and that derived
515   from the CAMS model.

Table 1 : TCCON stations used in this paper (Figure 4)

Stations	[lat ; lon]	Altitude [m]	Start Date	End Date	Reference
Wollongong	[-34.41 ; 150.88]	30	2008/06/26	2017/09/13	Griffith et al. 2017
Darwin	[-12.43 ; 130.89]	30	2005/08/28	2018/01/19	Griffith et al. 2017
Hefei	[31.90 ; 118.67]	30	2015/09/18	2016/12/31	Liu et al. 2018
Saga	[33.24 ; 130.29]	10	2011/07/28	2018/08/03	Shiomi et al. 2017
Pasadena	[34.14 ; -118.13]	240	2012/09/20	2018/10/01	Wennberg et al. 2017
Edwards	[34.96 ; -117.88]	700	2013/07/20	2018/10/01	Iraci et al. 2017
Tsukuba	[36.05 ; 140.12]	30	2011/08/04	2017/12/28	Morino et al. 2017
Lamont	[36.6 ; -97.49]	320	2008/07/06	2018/10/03	Wennberg et al. 2017
Parkfalls	[45.94 ; -90.27]	440	2004/06/02	2018/10/01	Wennberg et al. 2017
Zugspite	[47.42 ; 11.06]	2960	2015/04/24	2018/08/03	Sussmann and Rettinger 2017
Garmisch	[47.48 ; 11.06]	740	2007/07/16	2018/08/03	Sussmann and Rettinger 2017
Orleans	[47.97 ; 2.11]	130	2009/08/29	2017/12/31	Warneke et al. 2017
Paris	[48.85 ; 2.36]	60	2014/09/23	2018/01/26	Te et al. 2017
Karlsruhe	[49.1 ; 8.44]	110	2010/04/19	2018/10/22	Hase et al. 2017
Bremen	[53.10 ; 8.85]	7	2007/01/15	2018/01/09	Notholt et al. 2017
Bialystok	[53.23 ; 23.02]	180	2009/03/01	2017/12/13	Deutscher et al. 2017
Sodankyla	[67.37 ; 26.63]	190	2009/05/16	2018/10/03	Kivi et al. 2017

520

Appendix
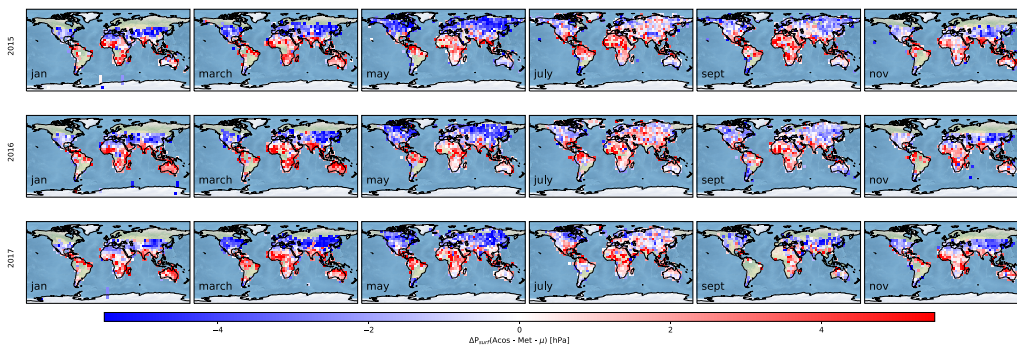
Figure A1 : Same as Figure 5 but for the surface pressure retrieved by the ACOS algorithm

525
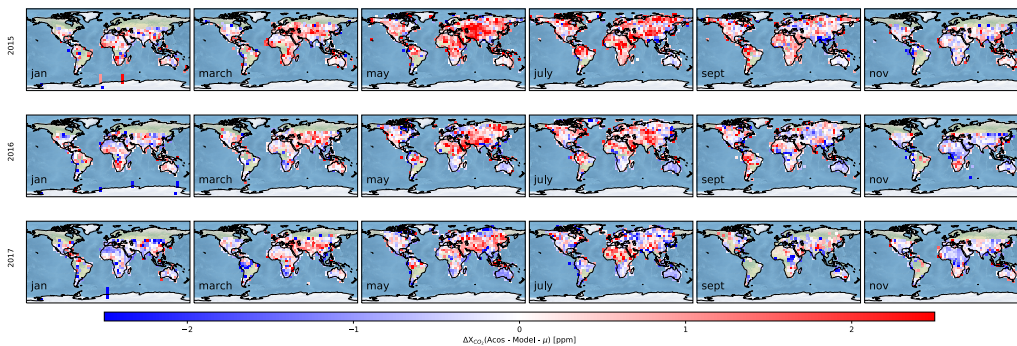
Figure A2 : Same as Figure 7 but for the XCO2 retrieved by the ACOS algorithm